Structure and morphology of coevaporated pentacene-perfluoropentacene thin films

A. Hinderhofer,[1] C. Frank,[2] T. Hosokai,[2] A. Resta,[2] A. Gerlach,[2] and F. Schreiber[2,a)]

[1]*Institut für Angewandte Physik, Universität Tübingen, Auf der Morgenstelle 10, 72076 Tübingen, Germany*
[2]*ESRF, BP 220, F-38043 Grenoble, France*

The structural properties of coevaporated thin films of pentacene (PEN) and perfluoropentacene (PFP) on SiO_2 were studied using x-ray reflectivity and grazing incidence x-ray diffraction. Reciprocal space maps of the coevaporated thin films with different volume fractions reveal the coexistence of two different molecular mixed PEN-PFP phases together with the pure PEN and PFP crystallites. The crystal structure of PEN:PFP blends does not change continuously with volume fraction, instead the proportion of the appropriate phases changes, as seen from the diffraction analysis. Additional temperature dependent experiments reveal that the fraction of the two mixed PEN-PFP phases varies with growth temperature. The λ-phase (molecular plane parallel to the substrate) is metastable and induced by low growth temperature. The σ-phase (molecular plane nearly perpendicular to the substrate) is thermally stable and nucleates predominantly at high growth temperatures. © *2011 American Institute of Physics*. [doi:10.1063/1.3557476]

I. INTRODUCTION

Blends of organic semiconductors are widely used in organic thin film devices, e.g., for charge carrier mobility improvement in organic field effect transistors[1] or for efficient charge carrier separation in photovoltaic bulk heterojunctions.[2–4] The mixing behavior in such multicomponent thin films used for devices is not well understood, because even the growth and structure of single-component thin films are already nontrivial.[5–9] Typically, a key question for such a mixed film is whether the materials are phase separating or mixing on the molecular level.

Complete or partial mixing of two molecular species might be possible, if a mixed crystal, which is energetically more favorable than two pure crystals exists. Of importance in this regard is the isostructural compatibility of both molecules, which is in many cases a prerequisite for efficient mixing.[10,11] A combination of compounds, whose molecular shape is rather different, often exhibits pronounced phase separation, which is the case for, e.g., mixtures of fullerene and Cu-phthalocyanine.[12] Generally, one expects that there are two driving forces for mixing or phase separation: First, the temperature dependent entropy term, which always favors complete mixing; second, the different interaction energies ($W_{A–A}$, $W_{B–B}$, $W_{A–B}$) between the molecules of species A and B, which can either favor or disfavor mixing.[10]

In thermal equilibrium at high temperatures, if all three interaction energies are similar, the mixing behavior is purely entropy-driven, leading to a continuously mixed crystal (solid solution)[10] where molecules of species A can randomly replace single molecules in a crystal of B [see in Fig. 1(a)]. Such a mixture would exhibit a continuous change of lattice constants dependent on the mixing ratio, which was reported, for example, in blends of different phthalocyanines.[3,13] In case that $W_{A–B}$ is very distinct from $W_{A–A}$ and/or $W_{B–B}$, we may find either phase separation [$W_{A–A}$ or $W_{B–B}$ large and attractive; Fig. 1(b)] or pronounced A–B pair formation in an ordered mixed crystal [$W_{A–B}$ large and attractive; Fig. 1(c)]. Blends of the latter kind are preferentially equimolar, and excess molecules would phase separate from the equimolar crystal [Fig. 1(d)].

In thin film growth nucleation of crystalline islands depends on the growth conditions, and is often kinetically limited and thus far from thermal equilibrium. Therefore, the above-mentioned conditions will not be completely fulfilled for thin film growth but rather constitute limiting cases.

An example of large energies $W_{A–B}$ due to electrostatic interactions is often found for blends of aromatic hydrocarbons and their perfluorinated counterparts.[14] Most of these blends form only equimolar mixed crystals.[14–16] Recently, it was shown that, under certain conditions, perfluoropentacene [$C_{22}F_{14}$, PFP; Fig. 1(e)][17,18] can form a molecular mixed crystal with its hydrogenated counterpart pentacene [$C_{22}H_{14}$, PEN; Fig. 1(e)].[19,20] Both PEN and PFP exhibit high charge carrier mobilities (PEN for holes, PFP for electrons) and high structural order in thin films.[21,22] Therefore, both molecules are candidates for an active layer in organic thin film devices[23,24] and interesting for fundamental studies of mixing behavior (phase mixing versus phase separation).

This paper intends to address two specific questions on the mixing behavior of PEN:PFP coevaporations. First, does the crystal structure of PEN:PFP blends change continuously with different mixing ratios or are there only specific mixed structures? Second, how does the mixing behavior change with growth temperature?
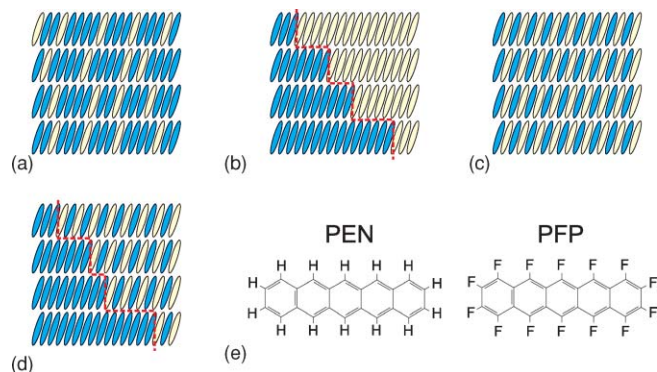
a)Electronic mail: frank.schreiber@uni-tuebingen.de.

FIG. 1. Sketches of possible mixing scenarios of a two component system: (a) Continuously mixed crystal, (b) phase separation, (c) ordered mixed crystal, (d) phase separation in a nonequimolar mixture with preferential A–B pair formation. Broken lines are highlighting phase boundaries. (e) Chemical structure of pentacene (PEN) and perfluoropentacene (PFP).
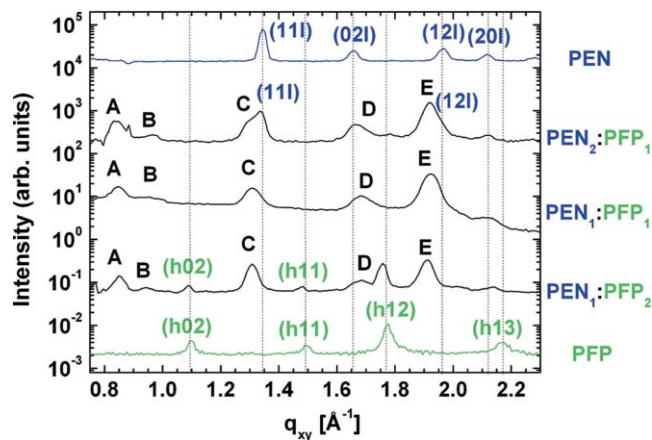

FIG. 2. GIXD data obtained from PEN:PFP coevaporations with different mixing ratios and from pristine PEN and PFP films. All films were grown at a substrate temperature of 300 K and have a thickness of 10–15 nm.

II. EXPERIMENTAL

Organic blends of PEN (Sigma Aldrich, 99.9% purity) and PFP (Kanto Denka Kogyo Co., 99% purity) were grown on silicon wafers covered by 1.3 nm native SiO_2 under ultra high vacuum conditions (base pressure $<5 \times 10^{-9}$ mbar) by thermal evaporation. The growth rate for both compounds was set to 0.1–0.2 nm/min monitored by a water-cooled quartz microbalance, which was calibrated via x-ray reflectivity. Substrate temperatures during growth were varied between $T = 250-330$ K with a combination of cooling by liquid nitrogen and heating by a resistive heater inside the sample holder.[25] Experiments with higher growth temperatures above 330 K were not performed since the higher desorption rate, especially of PFP, at higher temperatures would make it difficult to grow films with a defined mixing ratio.

Mixing ratios of PEN:PFP blends were checked post-growth by x-ray photoelectron spectroscopy. The F1/C1s intensity ratio can be related to the stoichiometry of the mixed film using the pure PFP and PEN spectra as a reference. The error in the mixing ratio was estimated to be less than 8%.

In situ grazing incidence x-ray diffraction (GIXD) measurements were performed with a point detector at beamline ID03 ($\lambda = 0.063$ nm) of the ESRF in Grenoble (France). Also at ID03 we used a MARCCD area detector (133 mm diameter) for producing reciprocal space maps (RSM) of several thin films. The maps show different areas of q-space, since the sample-detector distance was varied. For the transformation of the images from angular space to q-space the projection of the scattering signal onto the flat detector surface was neglected. Additional x-ray reflectivity and rocking scans were measured on a lab based x-ray diffractometer ($Cu_{K\alpha 1}$ radiation, multilayer mirror, double bounce compressor monochromator). Modeling and fitting of x-ray reflectivity data (XRR) were done with the MOTOFIT[26] software, which uses the Parratt formalism. Lower limits of coherent in-plane island sizes D were determined by the Scherrer formula $D = 2\pi/\text{FWHM} \cdot 0.9394 \cdot K_s$,[27] where $K_s = 1.0747$ is the Scherrer constant for spherical grains and FWHM is the full width half maximum of the peak.

Atomic force microscopy (AFM) images were measured in tapping mode within one week after film preparation with a JPK Nanowizard II.

III. RESULTS

A. Impact of mixing ratio on the structure of PEN:PFP coevaporated films

To test if the mixing ratio of PEN and PFP has an impact on the film structure, we compare GIXD data of blends with different molecular ratios [Fig. 2(a)]. Positions of Bragg reflections in q_{xy} based on the data in Fig. 2 are summarized in Table I.

For the 1:1 blend five in-plane Bragg reflections, which cannot be assigned to known structures of PEN and PFP, are observed (labeled "A" to "E"). The q_{xy}-values of these reflections are consistent with those reported in Ref. 19, indicating that the 1:1 film has no segregations and is completely mixed at the molecular level. Films with mixing ratios different from

TABLE I. Positions of GIXD Bragg reflections in q_{xy} from Fig. 2 for films with different PFP fraction. The error in the mixing ratio was estimated to be less than 8%.

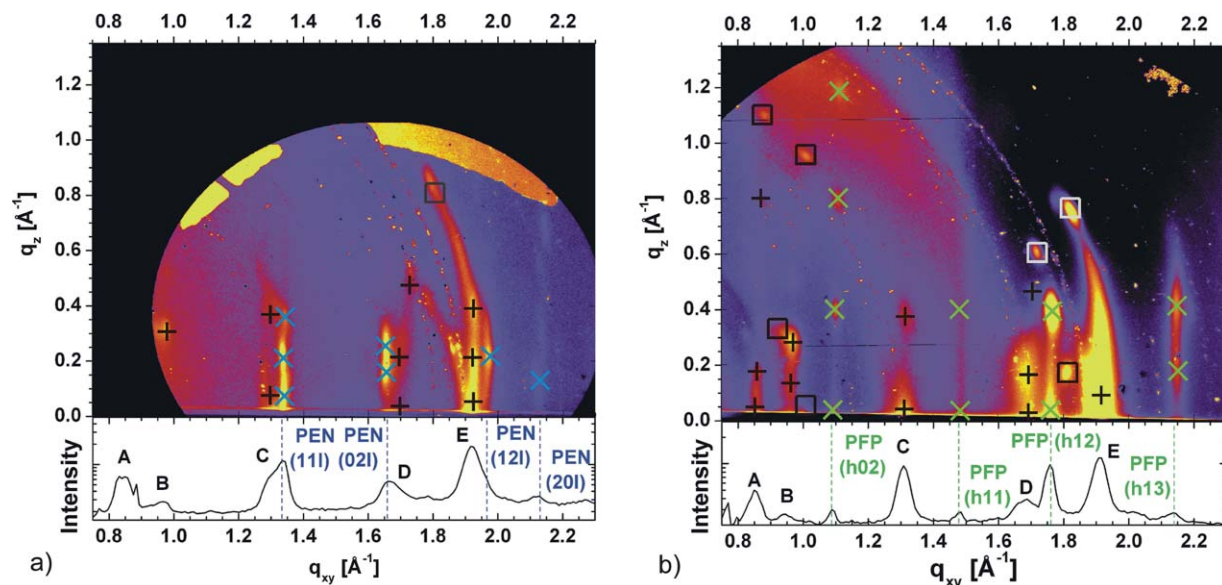| | q_{xy} positions [Å^{-1}] | | | | |
| | PFP fraction | | | | |
Reflection	0%	33%	50%	67%	100%
PFP (h02)	. . .	. . .	. . .	1.089	1.099
PFP (h11)	. . .	. . .	. . .	1.479	1.496
PFP (h12)	. . .	. . .	. . .	1.757	1.775
PEN (11l)	1.345	1.339	. . .	. . .	. . .
PEN (02l)	1.657	1.661	. . .	. . .	. . .
PEN (12l)	1.965	1.967	. . .	. . .	. . .
PEN (20l)	2.117	2.116	. . .	. . .	. . .
A	. . .	0.846	0.849	0.852	. . .
B	. . .	0.968	0.963	0.952	. . .
C	. . .	1.313	1.310	1.308	. . .
D	. . .	1.690	1.682	1.683	. . .
E	. . .	1.920	1.922	1.910	. . .

FIG. 3. Reciprocal space maps of two coevaporations (a) PEN_2:PFP_1 and (b) PEN_1:PFP_2 measured with a 2D detector. Additional data at the bottom of each picture are separate GIXD scans performed with a point detector at constant $q_z = 0.02$ Å^{-1}. Both films have a thickness of ~15 nm and were grown at $T = 330$ K. Labeling: green "×": PFP; blue "×": PEN; "+," and "□" mixed phases.

1:1, however, exhibit in-plane reflections of the pure PEN or PFP thin film structure, respectively, depending on the volume fraction. For example, in a PFP_2:PEN_1 blend the (h02), (h11), and (h12) reflections of the PFP thin film structure are at the same q_{xy} as in the pristine PFP film. PFP reflections are present neither in the PFP_1:PEN_1 nor in the PFP_1:PEN_2 blend. Likewise, the PEN (11l), (02l), and (12l) reflections appear only in PFP_1:PEN_2 and pure PEN films. Apart from small strain-induced shifts (~1%), PEN and PFP domains in the blends have unit cell parameters equal to their pristine film structures.[21,22] Additionally, in all blends with a mixing ratio differing from 1:1 we find reflections of the mixed phases at the same q_{xy}-position as in a 1:1 blend, indicating that the unit cell of the mixed film does not depend strongly on the mixing ratio. This coexistence of both pristine film structures and the 1:1 mixed film structures is a clear indication that the structure of PEN:PFP blends does not change continuously with the mixing ratio. This suggests that excess molecules of either species are phase separating in their own pure film structure similar to the sketch in Fig. 1(d).

Figure 3 shows in-plane reciprocal space maps of (a) PEN_2:PFP_1 and (b) PEN_1:PFP_2 films grown at $T = 330$ K. Additional GIXD data measured with a scintillation counter are shown at the bottom of Figs. 3(a) and 3(b). Here, crystal truncation rods of either the PFP or PEN thin film phase (marked by green and blue "×") are visible. Figure 3 also shows the complex structure of the mixed films: The in-plane diffraction features consist partly of textured rings and partly of diffuse crystal truncation rods. Features "B" and "D" at $q_{xy} = 0.96$ Å^{-1} and $q_{xy} = 1.92$ Å^{-1} consists of both a textured ring and a crystal truncation rod. The presence of diffraction features with a significant difference of mosaicity is a hint for structurally separated domains of different phases in the mixed film. Although an unambiguous assignment is very difficult we tried to distinguish between mixed film features with a large broadening in $|q|$ (marked by "□") and

features with a broadening in q_z direction (marked by "+"). When comparing Figs. 3(a) and 3(b) it is clear that features marked by "□" are less intense or even below the background. This observation may be attributed to preferred nucleation of this phase for PFP excess and a lower nucleation probability for an excess of PEN in the mixture. We tentatively assign the reflections marked by "□" in Figs. 3(a) and 3(b) to the λ-phase and the diffuse crystal truncation rods marked by "+" to the σ-phase.

From the GIXD peak width we determined the lower limit of coherently ordered in-plane island sizes for several coevaporated films (Table II). Coherent island sizes of the mixed structures are by a factor of ~2 smaller than the pure islands. This observation suggests that the in-plane long range order of the mixed structure is disturbed by many crystal defects compared to the structure of the pure films, which show well-defined crystal truncation rods in Figs. 3(a) and 3(b). In addition, the in-plane island size of the mixed structure does not critically depend on the mixing ratio. The coherently ordered domains of PEN and PFP in mixtures and in the pure films are nearly identical leading to the conclusion that the crystal growth of the pure film domains is not further disturbed by the presence of mixed domains nearby.

TABLE II. Average in-plane island sizes of PEN, PFP, and the mixed structure (σ-phase). The error in the mixing ratio was estimated to be less than 8%.

| | In-plane island size (nm) | | | | |
| | PFP fraction | | | | |
Structure	0%	33%	50%	67%	100%
PFP	...	...	...	25	21
Mixture (σ-phase)	...	11	11	14	...
PEN	20	20	...	...	...

B. Temperature dependence of 1:1 blends

X-ray reflectivity data [Fig. 4(a)] show that PEN_1:PFP_1 films consist of at least two mixed phases. The first two Bragg reflections, tentatively assigned as $(001)_\sigma$ and $(002)_\sigma$, are the first and second order reflections of a phase which consists of molecules with a standing orientation (σ-phase), since the lattice spacing is very similar to the PEN and PFP thin film structures, in which the molecules are also aligned with their long axis nearly perpendicular to the substrate. The lattice spacing of the σ-phase is $l_s = 1.578 \pm 0.005$ nm and was obtained by fitting the reflectivity data [Fig. 4(a)] with the Parratt formalism. In Ref. 19 a slightly different value of the σ-phase lattice spacing is reported (1.595 nm), which was obtained by fitting the peak maximum with a pseudo-Voigt profile and converting the result to a length l in real space via $q_z = 2\pi/l$. Our result is expected to be more precise, since due to superposition of the reflectivity signal with the Bragg reflection a certain shift
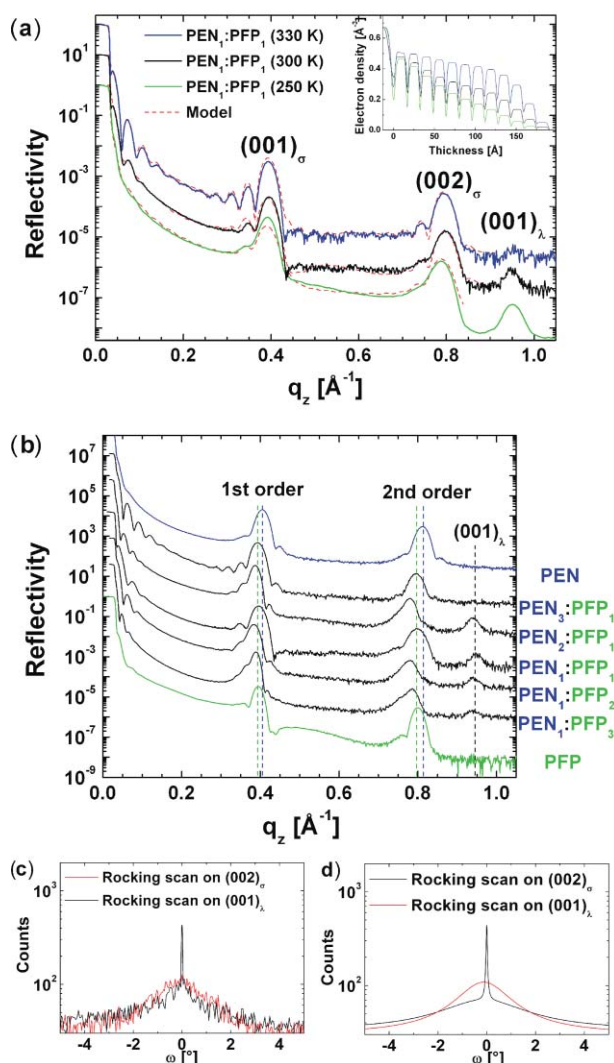
of the apparent peak maximum in q_z occurs, which can only be deconvoluted by a fit of the entire scan as performed here.

An additional Bragg reflection at $q_z = 0.951$ Å^{-1}, tentatively assigned as $(001)_\lambda$, corresponds to a lattice spacing of 0.66 ± 0.01 nm and probably stems from molecules with a more lying orientation relative to the substrate (λ-phase). The observation of mixed domains with two different structures is consistent with Ref. 19.

In Fig. 4(b) XRR data from different mixing ratios are shown for comparison. In general, all mixtures exhibit a first and second order diffraction peak corresponding to a structure with standing molecules. Apart from the PEN_3:PFP_1 film all mixtures exhibit a Bragg reflection for the λ-phase. This observation, together with the weak λ-phase features shown in Fig. 3(a), indicates that the λ-phase nucleation is weaker for films with large amounts of PEN, compared to mixtures with large PFP amounts. In addition, we find the peak maximum of the first and second order Bragg reflections of nonequimolar mixtures at lower q_z compared to the maximum of the equimolar mixture and the pure films. A direct conversion to real-space lengths would, therefore, indicate that the lattice spacing of the nonequimolar mixtures is larger in comparison to equimolar mixtures. However, for thin films exhibiting phase separation between several similar crystal structures on a scale smaller than the coherence length of the x-ray beam, interference between those structures is expected. The resulting intensity at a position in q_z is then strongly dependent on the exact spatial relation between the two crystal structures. Under these circumstances a direct conversion of q_z-coordinates from the peak-maximum into a real-space length can be misleading (see the Appendix for examples where the conversion will fail to give reasonable results). Therefore, we attribute the change in Bragg peak position for nonequimolar mixtures to interference effects between different phases and not to a change in lattice spacing.

Rocking scans on the $(002)_\sigma$ and $(001)_\lambda$ Bragg reflections for a 1:1 mixture grown at 300 K [Fig. 4(c)] show the mosaicity of both phases. Figure 4(d) shows fitting curves of the rocking scans by Lorentzian functions. The rocking scan on the $(002)_\sigma$ reflection consists of a sharp peak (FWHM $= 0.05 \pm 0.01°$) due to scattering under the Bragg condition and the broader diffuse background (FWHM $\sim 2.5°$). In the rocking scan on the $(001)_\lambda$ reflection the intensity of both the diffuse scattering and the Bragg scattering are superimposed with a similar FWHM $\sim 2.6°$. The large mosaicity of the λ-phase is consistent with the assignment of the reflections with large mosaicity in Figs. 3(a) and 3(b) (marked by "□") and the assignment of diffuse crystal truncation rods (marked by "+") to the σ-phase.

The relative intensity of the $(001)_\lambda$ reflection [Fig. 4(a)] shows a strong T dependence, implying that the fraction of λ-phase in a film depends crucially on T. The relative intensity of the $(001)_\lambda$ reflection is large at low temperatures ($T = 250$ K) and nearly vanishes at $T = 330$ K. This observation leads to the conclusion that the σ-phase (standing molecules) is thermally stable, whereas the λ-phase (lying molecules) is metastable and its nucleation is induced by low growth temperatures. Figure 5 shows a RSM of a 1:1 blend grown at $T = 250$ K. Only features from mixed phases (λ-phase and

FIG. 4. (a) XRR of three PEN_1:PFP_1 blends grown at different T. Peaks marked with the diffraction order and the phase as index. The inset shows the modeled electron density for each film. (b) XRR of films with different mixing ratio grown at 300 K. (c) Rocking scan on the $(002)_\sigma$ and $(001)_\lambda$ Bragg reflections of the PEN_1:PFP_1 (300 K) film. (d) Fit of rocking scans with Lorentzian functions.
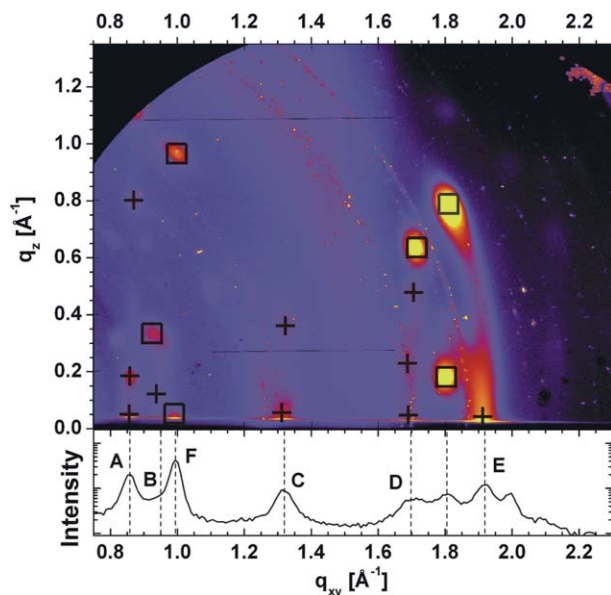
FIG. 5. Reciprocal space map of a 1:1 coevaporation grown at $T = 250$ K with a thickness of ~ 15 nm measured with a 2D detector. A separate GIXD scan performed with a point detector at constant $q_z = 0.02$ Å^{-1} is shown at the bottom. Labeling: "+": features assigned to the σ-phase; "□": features assigned to the λ-phase.

σ-phase) are visible, consistent with complete mixing of PEN and PFP on the molecular level. The relative intensities of features assigned to the λ-phase ("□") are increased compared to features assigned to the σ-phase ("+"), confirming the dominance of the lying phase at low T. In the GIXD data at the bottom of Fig. 5, a feature marked by "F" is the dominant reflection, which is weak in the high T films in Fig. 3.

From the peak positions in Table I, one may try to elaborate the in-plane lattice vectors of the σ-phase. We assign feature "A" to the (10l) reflection and "B" to the (01l) reflection. With an in-plane unit cell angle of $\gamma = 90°$, "C" would be the (11l) reflection, "D": (20l) and "E": (02l). Together with the out-of-plane lattice spacing of 1.575 nm the unit cell volume is $V = 760$ Å^3, which is intermediate the unit cell volumes of the pure materials crystal structures: $V_{PEN} = 697$ Å^3, $V_{PFP} = 816$ Å^3 (Refs. 19 and 22).

C. Roughness and morphology of PEN-PFP blends

To complement the x-ray diffraction data, AFM-images of PEN:PFP blends grown at different T are presented in Figs. 6(a)–6(c). They show that the surface of PEN:PFP blends exhibit two different morphologies: First, large terraces associated with the σ-phase, since the step height corresponds roughly to the spacing of one monolayer of the σ-phase; second, a network of needles associated with the λ-phase.[19] Films grown at $T = 300$ K [Fig. 6(a)] exhibit a significantly higher amount of the needle-shaped grains than films grown at $T = 330$ K [Fig. 6(b)]. This observation is consistent with x-ray reflectivity data, where an increase of the λ-phase for low temperatures is observed.

From AFM-images (Fig. 6) and from the electron density profiles shown in the inset of Fig. 4(a) it is evident that also the root-mean-squared roughness R of the mixed films varies
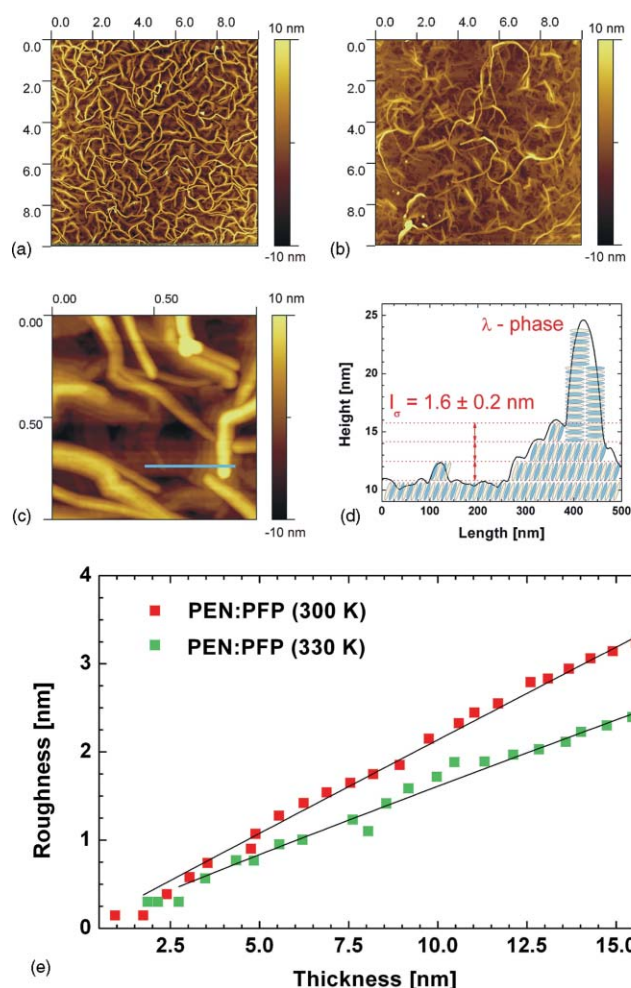

FIG. 6. AFM images (10×10 μm^2) of two PEN$_1$:PFP$_1$ coevaporations with a thickness of 16 nm grown at different T. (a) $T = 300$ K (b) $T = 330$ K. (c) Detailed view (1×1 μm^2) of the AFM image in (a). (d) Line scan with terrace height of the σ-phase. (e) Roughness versus film thickness of PEN$_1$:PFP$_1$ blends grown at different T. Black lines are fits with a power function.

with T. Table III shows roughness parameters extracted from the reflectivity data for different coevaporations (film thickness $d \sim 15$ nm). All coevaporations, regardless of the mixing ratio, exhibit a strong increase of R toward low T.

In addition, real-time x-ray reflectivity data measured during growth, allow the determination of R for each film thickness d.[8,28] Figure 6(e) shows a plot of R versus film thickness of PEN$_1$:PFP$_1$ blends grown at different T. The

TABLE III. Roughness values of PEN:PFP blends (~ 15 nm thickness) depending on growth temperature and mixing ratio. The error in the mixing ratio was estimated to be less than 8%.

	Roughness R (nm) PFP fraction		
Temperature [K]	25%	50%	75%
330	1.4	2.2	2.7
300	1.9	3.0	3.4
250	…	3.6	…

roughening of the low temperature film (300 K) is faster than the roughening of the high temperature film (330 K). Both roughness evolutions are fitted with an exponential function ($R \propto d^{\beta}$) to extract the growth exponent β.[29] The growth exponent of both films is nearly 1.0 ± 0.05, which is well beyond the growth exponent for random deposition ($\beta = 0.5$). This type of fast roughening ($\beta > 0.5$) was also observed for thermal deposition of other organic molecules.[30]

These findings reveal that the increased nucleation of the λ-phase coincides with faster roughening of PEN:PFP coevaporations at low T. A possible simplified rationalization of the fast roughening of the λ-phase compared to the σ-phase could go as follows: If the interaction energy between the conjugated π-systems of PEN and PFP is high, then stacking of molecules is most efficient in the direction, where the overlap of π-orbitals of PEN and PFP is large. This implies also fast grain growth in this direction. The stacking behavior of the σ-phase leads to flat terraces and "slow roughening" [Fig. 6(d)]. For the λ-phase, on the other hand, the molecular stacking is energetically favored in the direction perpendicular to the substrate, leading to "fast roughening." In Figs. 6(a) and 6(c) it is apparent that needles are mostly nucleating at the peaks of σ-phase terraces, as sketched in Fig. 6(d). In the roughness evolution of the PEN:PFP blends [Fig. 6(e)], we find no abrupt change leading to the conclusion that both growth modes are active in parallel in the observed regime.

IV. DISCUSSION

The finding of phase separation between the pure molecular domains and the 1:1 mixed domains raises the question whether other film properties in the blends, which are related to the film structure (optical and electrical), should change continuously with the mixing ratio or should reflect the behavior of a two or three component film with separated domains.

The electronic states of a blend depend on the domain size a of each phase and on the coupling length L, which is a characteristic length on which the molecular states are influenced by surrounding material. Note that the domain size a is not to be confused with the coherently ordered domain size D, which is always smaller than a. Then, there are two limiting cases for intermolecular coupling between adjacent patches of molecules. First, $a \gg L$: In this case, e.g., optical and ionization energy measurements would yield a superposition of domain specific physical characteristics (*large scale* phase separation). Second, $a \ll L$: For this condition molecular domains are small enough to allow a variation of molecular states due to intermolecular coupling (*small scale* phase separation). In the latter case, optical or ionization energy measurements would not yield a superposition of single component characteristics but would exhibit qualitatively new characteristics.

Salzmann *et al.*[31] reported that the ionization energy of PEN:PFP blends grown at room temperature changes continuously with the mixing ratio. The interpretation was partly based on the assumption that also the structure of PEN:PFP mixtures would continuously change with mixing ratio. Further, it was claimed that L is generally in the range of the

substrate-molecule distance, that is $L \sim 1$ nm. We showed, however, that the structure of PEN:PFP mixtures does not change continuously and that domain sizes a of such a blend are at least 10 nm, which corresponds to several unit cells (derived from the coherently ordered domain sizes, which are in the range of $D = 10$–20 nm for all phases). This would imply that domain sizes of $a \geq 10$ nm could be considered as *small scale* phase separation for PEN:PFP blends ($L > 10$ nm).

This inconsistency could be solved either by assuming that the coupling length in PEN-PFP blends is much higher then expected ($L \gg 10$ nm) or by re-interpretation of the experimental data in Ref. 31.

V. SUMMARY

The most important finding of this study is that PEN and PFP form a mixed crystal structure only for a 1:1 mixing ratio, probably due to a large interaction energy between PEN and PFP molecules. For other mixing ratios we found phase separation between the pure PFP or PEN structure and the two mixed 1:1 structures, as it is sketched in Fig. 1(d). Depending on the mixing ratio and growth temperature, each film consists of domains of four crystalline phases (PEN thin film, PFP thin film, 1:1 mixed λ-phase, and 1:1 mixed σ-phase). Therefore, a continuous change of lattice parameters of the mixed structure cannot be confirmed. Since a mixed crystal forms only for equimolar mixtures, we expect that the unit cells of the σ- and λ-phase contain an equal amount of PEN and PFP molecules.

Finally, the morphology and roughening of PEN:PFP blends were analyzed. Nucleation of the mixed λ-phase is induced by low T and growth of this phase leads to much faster roughening as compared to the growth of pure σ-phase.

APPENDIX: XRR SIMULATIONS FOR DIFFERENT MIXING BEHAVIORS

In a phase separating mixture of two crystal structures Bragg peak positions can be shifted due to interference between these structures. The exact characteristics of a reflectivity curve depend on the spatial relation of crystal grains in the film. Here, we discuss simulations of reflectivity curves for two examples of different phase separations to illustrate this issue: phase separation in the out-of-plane direction [inset Fig. 7(a)] and phase separation in the in-plane direction [inset Fig. 8(b)].

1. XRR simulations with out-of-plane phase separation

Relevant for XRR is the electron density in the q_z direction. For the simulation we choose a model with the following layers: Silicon substrate—four layers of the first material with a layer spacing of $l_s = 15.8$ Å and an electron
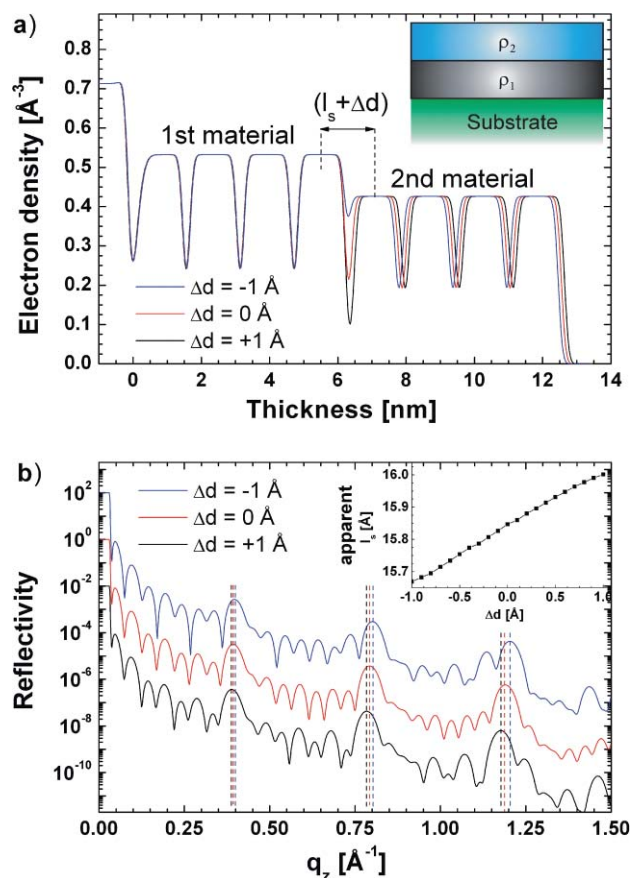
FIG. 7. (a) Simulated electron density profiles of a thin film with two different crystal structures. The inset shows a sketch of the sample structure. (b) Simulated XRR data from the electron densities shown in (a). The inset shows the dependence of the lattice spacing on the parameter Δd.
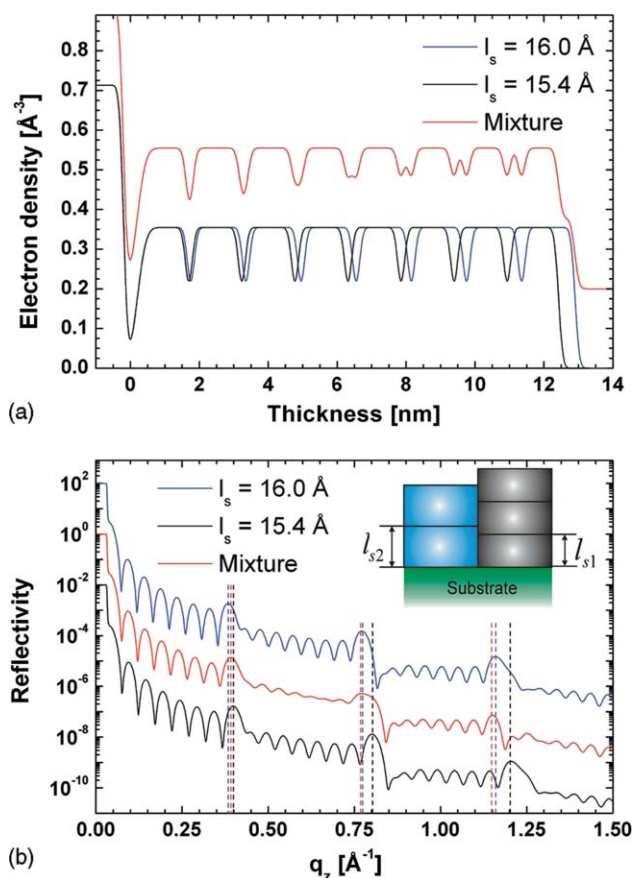

FIG. 8. (a) Simulated electron density profiles of two films with a different lattice spacing l_s and the electron density if these structures are mixed. For clarity the electron density of the mixture is shifted. (b) Simulated XRR data from the electron densities shown in (a). The inset shows a sketch of the mixed film with two lattice spacings.

density of $\rho_1 = 0.53$ Å^{-3}—four layers of a second material with $l_s = 15.8$ Å and $\rho_2 = 0.425$ Å^{-3}. An important parameter is the normalized distance $(1_s + \Delta d)$ between the first and the second material. In Fig. 7(a) electron density profiles are shown with different $\Delta d = \{-1; 0; 1\}$ Å, where for $\Delta d = 0$ the distance between the first and the second material is equal to the distance between two layers of a single material.

The Bragg peak positions in the corresponding reflectivity curves [Fig. 7(b)] are clearly shifted with respect to each other. The inset shows the dependence of the deduced apparent lattice spacing on the parameter Δd. This simulation shows that the Bragg peak positions in this case depend approximately linearly on Δd. The shift has a magnitude similar to the shift we observed for the nonequimolar PEN:PFP mixtures presented in Fig. 4(b).

2. XRR simulations with in-plane phase separation

In the case of lateral phase separation, we assume that the two crystal structures are growing on the substrate next to each other [inset in Fig. 8(b)]. For the simulation we assume that the two structures have the same electron density $\rho = 0.35$ Å^{-3} but different lattice spacings with $l_{s1} = 15.4$ Å and $l_{s2} = 16$ Å. The resulting electron density for a film with eight layers of the two structures and the mixture are shown

in Fig. 8(a). The resulting XRR curves [Fig. 8(b)] show that the Bragg peak maximum of the mixture would correspond to different lattice spacings dependent on diffraction order. For the second and third diffraction order, the Bragg peak maximum is at a lower q_z compared to both single crystal structures.

These two simulations illustrate that without exact knowledge of the microscopic spatial arrangement of the crystal structures in a phase-separated thin film Bragg peak positions in XRR cannot unambiguously be converted into a lattice plane spacing.

[1]K. Walzer, B. Maennig, M. Pfeiffer, and K. Leo, Chem. Rev. **107**, 1233 (2007).
[2]P. Peumans, S. Uchida, and S. R. Forrest, Nature (London) **425**, 158 (2003).
[3]A. Opitz, B. Ecker, J. Wagner, A. Hinderhofer, F. Schreiber, J. Manara, J. Pflaum, and W. Brütting, Org. Electron. **10**, 1259 (2009).
[4]J. Wagner, M. Gruber, A. Hinderhofer, A. Wilke, B. Bröker, J. Frisch, P. Amsalem, A. Vollmer, A. Opitz, N. Koch, F. Schreiber, and W Brütting, Adv. Funct. Mater. **20**, 4295 (2010).
[5]F. Schreiber, Phys. Status Solidi A **201**, 1037 (2004).
[6]G. Witte and C. Wöll, J. Mater. Res. **19**, 1889 (2004).
[7]S. Kowarik, A. Gerlach, and F. Schreiber, J. Phys. Condens. Matter **20**, 184005 (2008).

[8] B. Krause, F. Schreiber, H. Dosch, A. Pimpinelli, and O. Seeck, Europhys. Lett. **65**, 372 (2004).

[9] A. C. Dürr, N. Koch, M. Kelsch, A. Rühm, J. Ghijsen, R. L. Johnson, J.-J. Pireaux, J. Schwartz, F. Schreiber, H. Dosch, and A. Kahn, Phys. Rev. B **68**, 115428 (2003).

[10] A. I. Kitaigorodsky, *Mixed Crystals* (Springer, Berlin, 1984).

[11] J.-O. Vogel, I. Salzmann, S. Duhm, M. Oehzelt, J. P. Rabe, and N. Koch, J. Mater. Chem. **20**, 4055 (2010).

[12] A. Opitz, J. Wagner, W. Brütting, A. Hinderhofer, and F. Schreiber, Phys. Status Solidi A **206**, 2683 (2009).

[13] E. A. Lucia and F. D. Verderame, J. Chem. Phys. **48**, 2674 (1968).

[14] E. A. Meyer, R. K. Castellano, and F. Diederich, Angew. Chem., Int. Ed. **42**, 1210 (2003).

[15] S. Bacchi, M. Benaglia, F. Cozzi, F. Demartin, G. Filippini, and A. Gavezzotti, Chem.-Eur. J. **12**, 3538 (2006).

[16] F. Ponzini, R. Zagha, K. Hardcastle, and J. S. Siegel, Angew. Chem., Int. Ed. **39**, 2323 (2000).

[17] Y. Sakamoto, T. Suzuki, M. Kobayashi, Y. Gao, Y. Fukai, Y. Inoue, F. Sato, and S. Tokito, J. Am. Chem. Soc. **126**, 8138 (2004).

[18] A. Hinderhofer, U. Heinemeyer, A. Gerlach, S. Kowarik, R. M. J. Jacobs, Y. Sakamoto, T. Suzuki, and F. Schreiber, J. Chem. Phys. **127**, 194705 (2007).

[19] I. Salzmann, S. Duhm, G. Heimel, J. P. Rabe, N. Koch, M. Oehzelt, Y. Sakamoto, and T. Suzuki, Langmuir **24**, 7294 (2008).

[20] S. Kowarik, K. Broch, A. Hinderhofer, A. Schwartzberg, J. O. Osso, D. Kilcoyne, F. Schreiber, and S. R. Leone, J. Chem. Phys. **114**, 13061 (2010).

[21] S. Kowarik, A. Gerlach, A. Hinderhofer, S. Milita, F. Borgatti, F. Zontone, T. Suzuki, F. Biscarini, and F. Schreiber, Phys. Status Solidi (RRL) **2**, 120 (2008).

[22] S. Schiefer, M. Huth, A. Dobrinevski, and B. Nickel, J. Am. Chem. Soc. **129**, 10316 (2007).

[23] Y. Inoue, Y. Sakamoto, T. Suzuki, M. Kobayashi, Y. Gao, and S. Tokito, Jpn. J. Appl. Phys. **44**, 3663 (2005).

[24] T. Yokoyama, C. B. Park, T. Nishimura, K. Kita, and A. Toriumi, Jpn. J. Appl. Phys. **47**, 3643 (2008).

[25] K. A. Ritley, B. Krause, F. Schreiber, and H. Dosch, Rev. Sci. Instr. **72**, 1453 (2001).

[26] N. Andrew, J. Appl. Crystallogr. **39**, 273 (2006).

[27] M. Birkholz, *Thin Film Analysis by X-Ray Scattering* (Wiley, Weinheim, 2006).

[28] S. Kowarik, A. Gerlach, S. Sellner, F. Schreiber, L. Cavalcanti, and O. Konovalov, Phys. Rev. Lett. **96**, 125504 (2006).

[29] A.-L. Barabasi and H. E. Stanley, *Fractal Concepts in Surface Growth* (Cambridge University Press, Cambridge, 1995).

[30] A. C. Dürr, F. Schreiber, K. A. Ritley, V. Kruppa, J. Krug, H. Dosch, and B. Struth, Phys. Rev. Lett. **90**, 016104 (2003).

[31] I. Salzmann, S. Duhm, G. Heimel, M. Oehzelt, R. Kniprath, R. L. Johnson, J. P. Rabe, and N. Koch, J. Am. Chem. Soc. **130**, 12870 (2008).